Noise-induced interspike interval correlations and spike train regularization in spike-triggered adapting neurons

Eugenio Urdapilleta[1]

[1] *División de Física Estadística e Interdisciplinaria, Centro Atómico Bariloche, Av. E. Bustillo Km 9.500, S. C. de Bariloche (8400), Río Negro, Argentina*

arXiv:1610.09193v1 [q-bio.NC] 28 Oct 2016

PACS 87.19.ll – Models of single neurons and networks
PACS 87.10.Mn – Stochastic modeling
PACS 87.19.lc – Noise in the nervous system

Abstract –Spike generation in neurons produces a temporal point process, whose statistics is governed by intrinsic phenomena and the external incoming inputs to be coded. In particular, spike-evoked adaptation currents support a slow temporal process that conditions spiking probability at the present time according to past activity. In this work, we study the statistics of interspike interval correlations arising in such non-renewal spike trains, for a neuron model that reproduces different spike modes in a small adaptation scenario. We found that correlations are stronger as the neuron fires at a particular firing rate, which is defined by the adaptation process. When set in a subthreshold regime, the neuron may sustain this particular firing rate, and thus induce correlations, by noise. Given that, in this regime, interspike intervals are negatively correlated at any lag, this effect surprisingly implies a reduction in the variability of the spike count statistics at a finite noise intensity.

Introduction. – In many instances, point processes describing the firing statistics of different neurons go beyond the simple Poissonian declaration of temporal events or the more general renewal processes, which are often considered good descriptions of stationary spike trains [1–3]. Non-renewal firing properties have been observed in different species and neural areas [4–10]. The lack of independence between subsequent interspike intervals (ISIs), which defines the non-renewal character of a point process, may arise from different endogenous and exogenous mechanisms [11]. In particular, spike-evoked adaptation currents are one of the most prominent processes shaping the statistical structure of non-renewal spike trains [11–21].

Given that spikes constitute the main substrate for neuronal communication [1], these correlated events not only highlight the presence of certain history-dependent processes, but also imply profound effects on neural coding. For example, rate coding of static inputs is strongly affected by correlations between subsequent ISIs [22, 23], as well as the information transfer of slow signals [24, 25]. In particular, adaptation currents generally induce negative correlations, resulting in a long-term reduction of the variability of the spike count statistics [11–21], but richer patterns of correlations are also possible [20, 21].

Neurons respond to incoming stimuli in different ways. Type-I neurons or "integrators" are an important class of excitable neural cells, in which input signals are integrated up to a threshold, without any strong modulation by the spectral characteristics of fluctuations [26, 27]. For these neurons, it is important to differentiate two firing regimes: sub-threshold (or fluctuation/noise-driven) and supra-threshold (or input/mean-driven) modes [1, 28, 29]. Whereas in the first regime, neuronal dynamics has only a stable quiescent state and spiking responses can be reached only assisted by noise, in the second one, a repetitive firing is obtained even in a deterministic scenario and noise simply makes that trajectories fluctuate around a deterministic cycle. Different analytical studies have focused on the role of adaptation currents in generating interspike interval correlations in spike trains of neuron models set to the supra-threshold regime [19–21]. However, many cortical areas exhibit a fluctuation-sensitive or balanced regime [3, 30, 31], typically from a sub-threshold dynamics, and therefore, it would be important to assess the contribution of adaptation currents on the non-renewal characteristics of spike trains in this condition.

In this work, we address this analysis for the minimal

dynamical model supporting this phenomenon: the *leaky* integrate-and-fire (LIF) model. Two main approaches have been used to study correlations in integrate-and-fire (IF) models (although others can also be adapted): a method in which correlations are studied through the analysis of perturbations on a limit cycle [16, 20], and a method derived from the formulation of an appropriate hidden Markov model (HMM) [19, 23, 32]. The first method is extremely useful to study cases where adaptation produces realistic conditions, but it is restricted only to neuron models set in a repetitive firing regime, thus preventing its application to the analysis of the sub-threshold regime. By construction, the second method can be applied to any situation, but useful results were obtained analytically only for a perturbative regime of small adaptation currents [19]. Interestingly, both approaches result in correlations with essentially the same mathematical structure. Based on the second approach, here we study how interspike interval correlations behave in response to different features of the incoming stimuli, with particular emphasis in the noise-driven regime. Since previous studies have shown that a non-trivial structure of correlations arises as the firing rate of the spiking neuron is changed (by manipulating the deterministic drift, or an equivalent parameter) [12, 14–16, 19–21], we hypothesize that a similar situation can be reached, in the sub-threshold regime, when noise varies, by setting the firing rate at selected values. Confirming this hypothesis, we found that, in any sub-threshold regime defined by a fixed drift, negative correlations are maximal at a finite noise, implying a surprising regularizing effect of noise on long-term spike count variability. Further studies on the consequences of this effect are under analysis.

Simplified neuron models with spike-evoked adaptation. – Single-cell neuronal models describe the electrical properties of voltage-sensitive membranes, including their response to incoming signals. Often, integration of signals produces stereotyped spikes when the transmembrane potential reaches certain value or threshold. Initiated by the foundational description of the excitability of the squid axon by Hodgkin and Huxley in 1952, conductance-based models characterizing the behavior of ionic channels and their interaction with the membrane potential account not only for this highly nonlinear process of spike generation [1], but also for many other subthreshold phenomena including oscillations [33] or adaptation with subthreshold activation [14, 34], among others. Unlike high-dimensional detailed models, IF neuronal models are approximate descriptions that relieve the need of a precise spike generation mechanism and simply produce spikes by declaration. However, in order to keep as much information as possible between spikes, the description of the electrical evolution of the potential during the subthreshold period should include all relevant phenomena. For type-I neurons, the LIF model can be considered as the minimal model preserving the characteristics of neuronal processing during rest (leaky current and asymptotic relaxation).

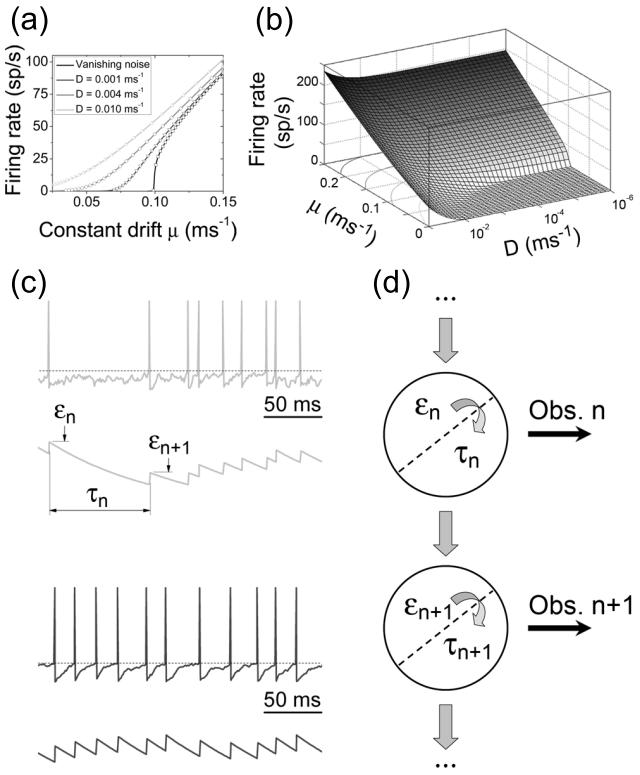

Fig. 1: The LIF neuron model and the hidden Markov correlated sequence of ISIs. (a) Firing rate response of a LIF neuron as a function of the constant drift driving the dynamics, μ, for different noise intensities, D. (b) Firing rate response as a function of μ and D. Parameters: $V_{\rm r} = 0$, $V_{\rm thr} = 1$, $\tau_{\rm m} = 10$ ms, $\alpha = 0$ (no adaptation). (c) Simulated voltage trace and adaptation current in the sub-threshold (upper figures, light-gray lines) and the supra-threshold (lower figures, dark-gray lines) regimes. Variables defining the HMM used for the analysis of correlations between ISIs are indicated. (d) Hidden Markov model: the statistics of the $(n+1)$-th observation (ISI), τ_{n+1}, is conditioned to the $(n+1)$-th initial adaptation level, ε_{n+1}, which in turn only depends on both variables at the immediately previous stage.

Neuronal adaptation includes a variety of interrelated processes, from spike-triggered and subthreshold-activated adaptation currents [14] to multi-time-scale adaptation [35,36]. The addition of a spike-evoked adaptation current gives a more realistic description to IF models (including a physiological basis of the widespread phenomenon of *spike-frequency adaptation*), without a substantial increase of complexity. In detail, we consider that, during subthreshold integration, the membrane potential evolves according to

$$\frac{dV}{dt} = -\frac{(V - V_{\rm rest})}{\tau_{\rm m}} + I_{\rm adapt} + \mu + \xi(t), \qquad (1)$$

where the time constant given by the leaky current is $\tau_{\rm m}$, the resting potential is $V_{\rm rest}$, the adaptation current is de-

noted by $I_{\rm adapt}$, and the external signal is represented by the constant drift μ. Randomness arises at different stages during signal transduction and neuronal communication [37], and here it is included simply as an additive Gaussian white noise, $\langle\xi(t)\rangle = 0$ and $\langle\xi(t)\xi(t')\rangle = 2D\delta(t'-t)$. This dynamics governs the evolution of the membrane potential during the subthreshold integration; whenever the potential reaches a certain threshold $V_{\rm thr}$, a spike is produced (or declared) and immediately after, the potential is set to a reset value $V_{\rm r}$. By a simple re-scaling of V, we can consider $V_{\rm rest} = 0$ and $V_{\rm thr} = 1$ without loss of generality. Furthermore, for simplicity we define $V_{\rm r} = V_{\rm rest} = 0$.

One of the most important output properties of a spiking neuron is its firing rate, i.e., the number of spikes produced in certain time. When analyzed as a function of an input feature, the resulting *tuning* function represents a input-output mapping, which usually is modulated by different factors. For the deterministic LIF model, spikes can be produced only when the constant drift is above certain value, see fig. 1(a), which separates two different regimes: sub- and supra-threshold regimes. This discontinuous mapping is monotonically smoothed by noise, see figs. 1(a) and 1(b). In the subthreshold mode, the input drift drives the neuronal dynamics towards a quiescent state below the potential threshold, see fig. 1(c) (upper trace in light-gray line), and noise is essential to produce any spike. In the supra-threshold mode, the dynamical state is set to a repetitive firing regime, see fig. 1(c) (lower trace in dark-gray line), and noise has no such a fundamental role. Interestingly, a given firing rate can be obtained in both regimes by proper combinations of input parameters, (μ, D), see fig.1(b).

A spike-evoked adaptation current mimics the effects of $Ca^{2+}-$activated K^+ or *after-hyperpolarization* currents [38], which are widely expressed in the mammalian nervous system [39], and can be minimally modelled by a current-based description [12, 15, 19, 40], $I_{\rm adapt}(t) = -g_{\rm adapt}\, x(t)$, where the adaptation process $x(t)$ filters the output spike train according to

$$\frac{dx}{dt} = -\frac{x}{\tau_{\rm a}} + \alpha \sum_i \delta(t - t_i). \tag{2}$$

In this equation, $\tau_{\rm a}$ and α define the temporal and the output scales of the adaptation process, respectively, and $\delta(t_i)$ is a pulse (Dirac delta function) representing a spike occurring at time t_i. Without loss of generality [19], $g_{\rm adapt}$ can be conveniently re-scaled so the temporal profile of the adaptation current during the input integration of the n-th interspike interval, $\tau_{\rm n} = t_{\rm n+1} - t_{\rm n}$, reads

$$I_{\rm adapt} = -\frac{\varepsilon_{\rm n}}{\tau_{\rm a}} \exp[-(t - t_{\rm n})/\tau_{\rm a}]. \tag{3}$$

Coupling between successive initial adaptation strengths is provided by integration of eq. (2) during the arrival of a new spike,

$$\varepsilon_{\rm n+1} = \varepsilon_{\rm n} \exp(-\tau_{\rm n}/\tau_{\rm a}) + \alpha, \tag{4}$$

see fig. 1(c). As depicted schematically in fig. 1(d), the preceding relationship supports a history-dependent process that creates correlations between subsequent ISIs [19]. The statistics of the $(n+1)$-th ISI, $\tau_{\rm n+1}$, is conditioned to the level of the $(n+1)$-th initial adaptation strength, $\varepsilon_{\rm n+1}$, through a temporally inhomogeneous first-passage-time problem with an exponential time-dependent drift [41–43]. Furthermore, since the initial adaptation strength of the $(n+1)$-th period depends exclusively on both variables at the immediately previous stage, $\varepsilon_{\rm n}$ and $\tau_{\rm n}$, through eq. (4), this scheme constitutes a Markov process with both an observable (interspike interval) and a hidden variable (initial adaptation strength). However, correlations between ISIs are not limited to consecutive periods, but extends to all previous outcomes, due to a nested dependence via the hidden variable. A similar HMM can be defined for other history-dependent processes that also produce spike-frequency adaptation and generate correlations between ISIs [17, 32, 44].

Correlations in the sequence of interspike intervals. – To quantify these correlations it is useful to define the serial correlation coefficient (SCC), which, in stationary conditions, is given by

$$\rho_{\rm k} = \frac{\langle \tau_{\rm n}\tau_{\rm n+k}\rangle - \langle\tau\rangle^2}{\langle(\tau - \langle\tau\rangle)^2\rangle}, \tag{5}$$

where brackets denote ensemble average and k is the lag between successive ISIs. To compute the SCCs at any lag, it is necessary to quantitatively describe the HMM depicted in fig. 1(d). Given the deterministic update defined by eq. (4), this HMM is completely characterized by the transition probability density

$$f(\varepsilon_{\rm n}, \tau_{\rm n}|\varepsilon_{\rm n-1}, \tau_{\rm n-1}) = \delta\{\varepsilon_{\rm n} - [\varepsilon_{\rm n-1}\exp(-\tau_{\rm n-1}/\tau_{\rm a}) + \alpha]\} \times \phi(\tau_{\rm n}|\varepsilon_{\rm n}), \tag{6}$$

where $\phi(\tau_{\rm n}|\varepsilon_{\rm n})$ is the ISI probability density for the (temporally inhomogeneous) system defined by eqs. (1) and (3) evolving from the reset to the threshold, conditioned to the explicit knowledge of the initial strength $\varepsilon_{\rm n}$. Recently, we showed that this probability density can be expressed as a series expansion in terms of the initial strength of the adaptation current for any one-dimensional IF model,

$$\phi(\tau|\varepsilon) = \sum_{\rm n=0}^{\infty} \varepsilon^{\rm n}\ \phi_{\rm n}(\tau), \tag{7}$$

and, particularly, we explicitly computed all terms for the LIF model [43].

Based on the transition probability defined by eq. (6), in a previous work [19], we computed $\langle\tau_{\rm n}\tau_{\rm n+k}\rangle$ and $\rho_{\rm k}$, assuming that the statistics given by eq. (7) and all nested expressions produced when computing SCCs at higher lags are developed up to order 1. In this small adaptation scenario (set by small values of α), correlations for any IF model develop a geometrical structure,

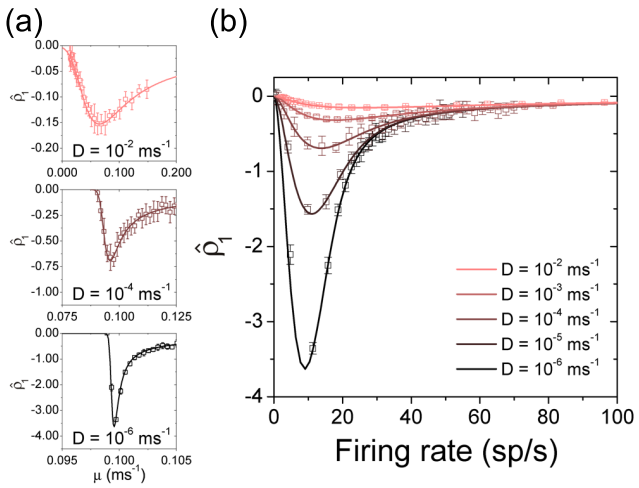

Fig. 2: (Color online) Normalized SCC at lag 1, $\hat{\rho}_1 = \rho_1/\alpha$, when spiking rate responses are set by the drift μ. (a) $\hat{\rho}_1$ as a function of the constant input μ driving the neuron, for different noise intensities. Analytical expressions (colored lines) and correlations obtained from the simulated dynamics (corresponding symbols, each calculated from a sequence of $N = 10^6$ ISIs) show an excellent agreement. (b) $\hat{\rho}_1$ represented as a function of the firing rate, for different noise intensity scenarios. Interestingly, the largest absolute value is reached at approximately the same firing rate in all cases. Parameters: Same as in fig. 1, except that $\alpha = 0.01$ in simulations and $\tau_a = 100$ ms.

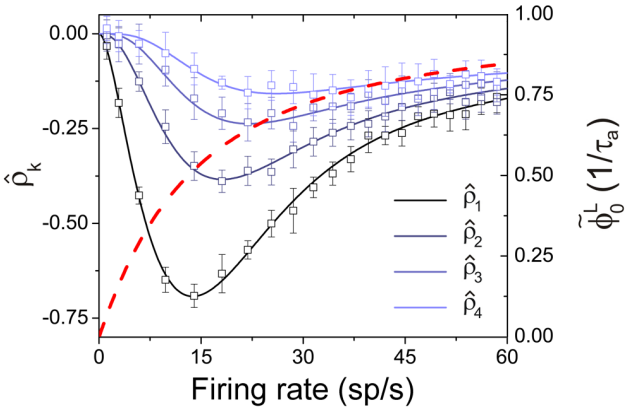

Fig. 3: (Color online) Normalized SCCs at higher lags, $\hat{\rho}_k = \rho_k/\alpha$. Analytical expressions (bluish colored lines) perfectly agree with data obtained from simulations (corresponding symbols, each calculated from a sequence of $N = 5 \times 10^6$ ISIs). The factor defining the geometrical structure, $\tilde{\phi}_0^L(1/\tau_a)$, is also shown (red dashed line, scale on the right side). As in fig. 2, firing rate was determined by varying the constant drift μ. Parameters as in fig. 2, with $D = 10^{-4}$ ms^{-1}.

$$\rho_k = \left[\tilde{\phi}_0^L(1/\tau_a)\right]^{k-1} \rho_1, \tag{8}$$

where $\tilde{\phi}_0^L(s)$ is the Laplace transform of the ISI density function for the unperturbed system (i.e., without the adaptation current), and ρ_1, the first SCC, reads

$$\rho_1 = -\alpha \frac{\langle\tau\rangle_{\phi_1}}{\left[1-\tilde{\phi}_0^L(1/\tau_a)\right]\langle(\tau-\langle\tau\rangle)^2\rangle_{\phi_0}} \times \left[\tilde{\phi}_0^L(1/\tau_a)\,\langle\tau\rangle_{\phi_0} + \frac{d\tilde{\phi}_0^L(s)}{ds}\Big|_{1/\tau_a}\right]. \tag{9}$$

The indexed brackets in eq. (9) are the contributions to the moments computed with the functions indicated by the respective index,

$$\langle\tau\rangle_{\phi_n} = \int_0^\infty \tau\,\phi_n(\tau)\,d\tau = -\frac{d\tilde{\phi}_n^L(s)}{ds}\Big|_{s=0}. \tag{10}$$

Therefore, within this framework, the two quantities needed to evaluate all SCCs are the unperturbed ISI density function (expressed in the Laplace domain) $\tilde{\phi}_0^L(s)$ and the first order correction $\tilde{\phi}_1^L(s)$ (or, at least, its effect on the mean ISI, $\langle\tau\rangle_{\phi_1}$). For the LIF model, these quantities read

$$\tilde{\phi}_0^L(s) = e^{-(Z_{thr}^2 - Z_r^2)/4}\,\frac{\mathcal{D}_{-\tau_m s}(Z_r)}{\mathcal{D}_{-\tau_m s}(Z_{thr})}, \tag{11}$$

$$\tilde{\phi}_1^L(s) = \frac{\sqrt{\tau_m/D}}{1-\tau_d/\tau_m}\,\frac{e^{-(Z_{thr}^2 - Z_r^2)/4}}{\mathcal{D}_{-\tau_m s}(Z_{thr})}\,s\left[\mathcal{D}_{-\tau_m(s+1/\tau_m)}(Z_r) - \frac{\mathcal{D}_{-\tau_m(s+1/\tau_m)}(Z_{thr})}{\mathcal{D}_{-\tau_m(s+1/\tau_d)}(Z_{thr})}\,\mathcal{D}_{-\tau_m(s+1/\tau_d)}(Z_r)\right], \tag{12}$$

where $Z_i = \sqrt{\tau_m/D}\,(\mu - V_i/\tau_m)$, and $\mathcal{D}_\nu(z)$ is the parabolic cylinder function according to Whittaker's notation [45].

In fig. 2(a) we show the first SCC (normalized by α), which sets the basis for all other SCCs at higher lags, as a function of the constant input driving the spiking dynamics, μ, for different noise intensities. When ρ_1 is represented as a function of the firing rate elicited by the constant input, fig. 2(b), we can observe that the behavior is approximately conserved, but scaled, across the different cases. Importantly, irrespective of the noise intensity, ρ_1 exhibits a minimum around certain firing frequency.

The geometrical structure of the SCCs at higher lags, eq. (8), depends on a scaling factor given by the ISI density function of the system without adaptation, $\phi_0(\tau)$, but Laplace-transformed and evaluated at a specific value, $\tilde{\phi}_0^L(1/\tau_a)$. In fig. 3 we show the first 4 correlation coefficients, for a representative case, as a function of the firing rate elicited by varying the constant input current, μ. The scaling factor is shown in red dashed line, whose scale can be read on the right margin. Given the monotonic character of this scaling factor, successive minima slightly shift towards higher firing rates as lag increases.

Noise-induced correlations. – Overall, the preceding results are very similar to those we have previously obtained for a *perfect* IF (PIF) neuron model [19]. In this

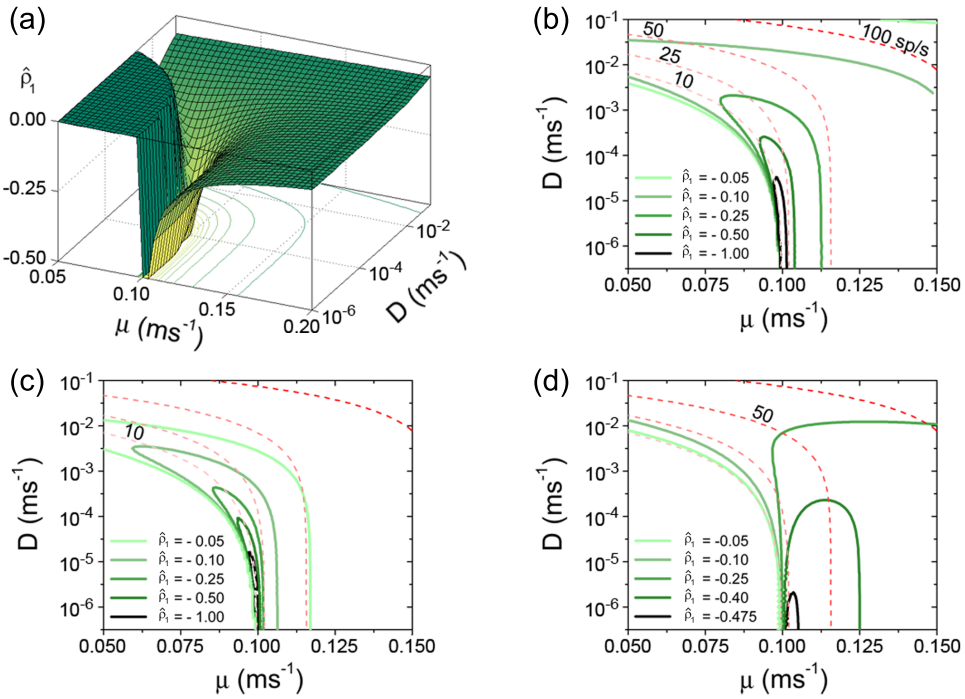

Fig. 4: (Color online) Structure of correlations. (a) Normalized SCC at lag 1, $\hat{\rho}_1$ in parameter space. A deep valley approximately follows the trajectory of the isoline corresponding to a specific firing rate (compare normalized SCC isolines at the bottom plane with firing rate isolines in fig. 1(b)). (b) Bi-dimensional representation of the contour structure. Greenish lines represent contours of $\hat{\rho}_1$ (indicated in the inset), whereas reddish dashed lines are isolines of firing rates (indicated *in situ*). Correlation contours approximately follow the isoline corresponding to 10 sp/s (i.e., $\sim 1/\tau_a$). Parameters for (a) and (b): same as in fig. 2, including $\tau_a = 100$ ms. (c) The structure of correlations develops narrowly around a lower firing rate (~ 2 sp/s) when time scale of the adaptation current is increased ($\tau_a = 500$ ms). (d) The opposite is true when time scale is reduced. Overall, correlation weakens (see inset) and develops loosely around the indicated firing rate. In this case, $\tau_a = 20$ ms and ~ 50 sp/s.

study, we have shown the same behavior, but analyzed as a function of the constant input μ, which actually is equivalent to the firing rate but scaled (in the pure PIF model, noise does not modulate the firing rate). Even when it is useful to gain theoretical insight with a tractable model, the PIF model lacks of biological realism, as it only can be set in the supra-threshold regime and noise simply randomizes spike times without any fundamental role. Here, with the study of the LIF model, we can focus on the subthreshold regime and analyze the contribution of noise in creating correlations.

Given that, according to fig. 2(b), minima of correlations for different cases are set around certain firing rate, the key idea to explore is whether there is a matching of time scales between the adaptation process, which is the responsible for creating correlations, and the firing state. In fig. 4(a) we show the first SCC in the input parameter space, μ and D. In the low-noise limit, it can be observed a deep valley, characterized by the value of μ that elicits a particular firing rate. As noise increases, the position of this valley moves along, bending towards the D-axis. If we focus on the contour levels, we can distinguish that ρ_1-isolines are similar to those of the firing rate, see fig. 1(b), implying that the development of strong correlations are concomitant to a particular firing rate. This is further developed in fig. 4(b), where the contour levels of ρ_1 and the firing rate are plotted together in the parameter space. As a general trend, correlations are structured around 10 sp/s, which tentatively corresponds to $1/\tau_a$. Since the adaptation process is the responsible for creating a history-dependent spike train, its time constant sets the scale in which spikes should be produced to maximize the influence of the update rule, eq. (4), on the development of correlations. Therefore, by changing the adaptation time constant we should observe that correlations develop around a different contour level of the firing rate. This scenario is shown in figs. 4(c) and 4(d), where adaptation time scale has been set at $\tau_a = 500$ ms and $\tau_a = 20$ ms, respectively. As expected, correlations organize around 2 sp/s (shown as below 10 sp/s) and 50 sp/s, respectively, with the additional effect that they are strengthened (weakened) as adaptation time scale increases (decreases).

The preceding observation corresponds to a matching of time scales: for a given adaptation process (a defined τ_a), correlations are stronger when the neuron fires at a certain firing rate. In particular, this firing rate can be elicited in a subthreshold regime and, furthermore, be driven by noise. In this case, for example, the constant input μ may be fixed by external influences and noise can be considered as a parameter. Different cases, corresponding to different

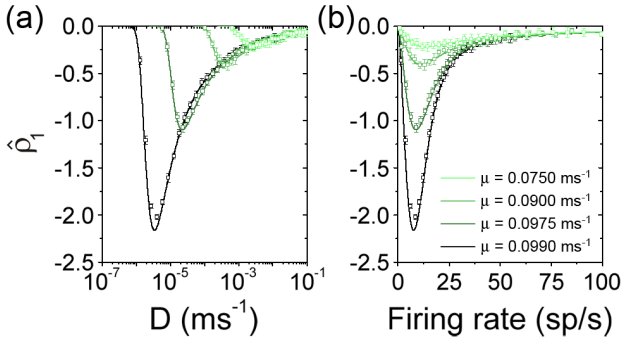

Fig. 5: (Color online) Noise-induced correlations. (a) Normalized SCC at lag 1, $\hat{\rho}_1$, as a function of the noise intensity, for different sub-threshold scenarios (established by μ). The transition to the supra-threshold condition occurs at $\mu = 0.100$ ms^{-1} (parameters as in fig. 2). Greenish lines represent analytical expressions, whereas corresponding symbols are data obtained from simulations (each data-point was calculated from a sequence of $N = 5 \times 10^6$ ISIs). Extreme correlations occur at a finite noise, whose value depends on the specific sub-threshold case. (b) When represented as a function of the ongoing firing rate, all minima are set around the same rate, indicative of a matching of time scales sustained by noise.

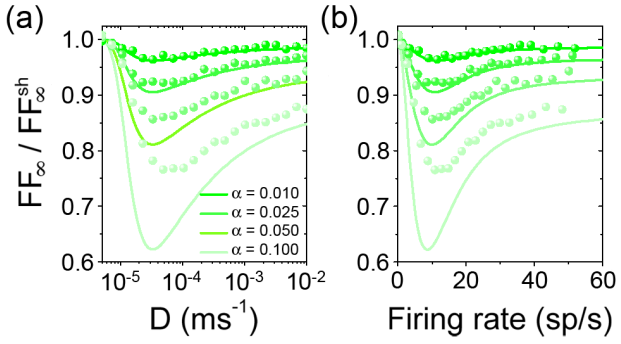

Fig. 6: (Color online) Spike train regularization by negative correlations. (a) Ratio between the Fano factor and the Fano factor of a surrogate spike train with ISI correlations removed by shuffling, $\mathrm{FF}_\infty/\mathrm{FF}^{\mathrm{sh}}_\infty$, as a function of the noise intensity, for a LIF neuron model set in a subthreshold regime (symbols). This ratio highlights the exclusive contribution of correlations on the reduction of the spike-train variability, $1 + 2\ \sum_{\mathrm{k}=1}^{\infty} \rho_{\mathrm{k}}$ (lines). Temporal windows used to compute spike-counts were large enough to assure asymptotic conditions. Parameters as in fig. 2, with $\mu = 0.0975$ ms^{-1}. Different contributions of the adaptation current to the dynamics are considered, see different values of α. (b) When represented as a function of the evoked firing rate, the strongest reduction of the spike-count variability is observed at a particular firing rate.

values of μ, are shown in fig. 5(a). The closer the value of μ to the critical value separating sub- and supra-threshold regimes (here, 0.10 ms^{-1}), the stronger the correlations and, of course, the weaker the noise intensity that maximizes them. However, as we argue above, the intrinsic phenomenon is a matching of time scales, so when represented as a function of the firing rate elicited by the noise, see fig. 5(b), all cases display their maximum of correlations at the same firing rate. From a different perspective, for a given system (i.e., a defined τ_{a} and D), there will be certain subthreshold external input μ that produces the strongest negative correlations (sustained by noise).

A minimum in the first SCC as a function of the noise intensity was previously reported for a related model [32]. In this study, the authors have numerically found a shallow minimum in ρ_1 at a finite noise, for a LIF neuron model with a history-dependent threshold. This minimum was not very pronounced probably because the system was set in the supra-threshold regime. At the light of our results, a precise value of the noise intensity will be influential only in a sub-threshold condition.

Influence on spike-count statistics. – The development of correlations between ISIs has an important impact on rate coding. In general, the *Fano factor* is utilized to characterize the relative importance of the first two moments of the statistics defined by the number of spikes observed in a temporal window of length T, as $\mathrm{FF}_T = \langle \Delta n_T^2 \rangle / \langle n_T \rangle$, where $\langle n_T \rangle$ and $\langle \Delta n_T^2 \rangle$ are the mean and the variance, respectively. For $T \to \infty$, the Fano factor converges to [22]

$$\mathrm{FF}_\infty = \lim_{T\to\infty} \mathrm{FF}_T = \mathrm{CV}^2 \left(1 + 2 \sum_{\mathrm{k}=1}^{\infty} \rho_{\mathrm{k}}\right), \qquad (13)$$

where CV is the *coefficient of variation*, defined on the statistics of single ISIs as $\mathrm{CV} = \sqrt{\langle \Delta\tau^2 \rangle}/\langle \tau \rangle$.

Therefore, a process that creates negative correlations also generates a reduction of the spike-count variability, as the factor $1 + 2\ \sum_{\mathrm{k}=1}^{\infty} \rho_{\mathrm{k}}$ is less than unity. These correlations can be removed from a spike train by *shuffling* the order of the ISIs, a procedure that creates a surrogate spike train with exactly the same single ISI statistics, but no correlations between them. Then, the ratio $\mathrm{FF}_\infty/\mathrm{FF}^{\mathrm{sh}}_\infty$ clearly highlights the exclusive contribution of correlations in the reduction of the spike-count variability. In fig. 6(a) we show this reduction as a function of the noise intensity, in a given subthreshold regime. When represented as a function of the firing rate evoked, fig. 6(b), the strongest reduction of the spike-count variability is positioned at the firing rate that matches the adaptation process (10 Hz).

In fig. 6, we can observe that our analytical derivation perfectly agrees to numerical results in the perturbative regime (brighter green symbols), where this framework is valid, whereas higher order effects on correlations are visible when α increases (dimer green symbols). Clearly, these effects have to oppose the linear decrease in order to prevent an unlimited growth beyond physical significance. However, the conclusion that a reduction of the spike-count variability and, therefore, a regularization of the spike train is maximized at a specific firing frequency

(here, sustained by a specific value of noise intensity) holds well beyond the perturbative scenario, indicating that the effect subsists in more realistic adaptation conditions.

Conclusions. – In this work we have analyzed the development of negative correlations in a LIF neuron model with a spike-triggered adaptation current. This system is adequate to explore both supra- and sub-threshold regimes. Whereas the first regime has been previously studied, and also confirmed by the present approach, the second one has been never characterized. We found that correlations are stronger as the neuron fires at a particular firing rate, defined by the inverse of the adaptation time scale. Obviously, this scenario can be obtained in both firing regimes, and when restricted to the sub-threshold case, noise plays a fundamental role, by driving the specific firing rate that maximizes correlations. Given that the sum of negative correlations at different lags produces a regularization of the long-term spike-count variability [13, 19, 22], this noise-sustained effect implies that noise may have a constructive role in neural rate codes when adaptation currents are present.

* * *

This work was supported by the Consejo de Investigaciones Científicas y Técnicas de la República Argentina.

REFERENCES

[1] Gerstner W., Kistler W. M., Naud R. and Paninski L., *Neuronal dynamics: From single neurons to networks and models of cognition* (Cambridge University Press, Cambridge) 2014.
[2] Perkel D. H., Gerstein G. L. and Moore G. P., *Biophys. J.*, **7** (1967) 391.
[3] Shadlen M. N. and Newsome W. T., *J. Neurosci.*, **18** (1998) 3870.
[4] Lowen S. B. and Teich M. C., *J. Acoust. Soc. Am.*, **92** (1992) 803.
[5] Ratnam R. and Nelson M. E., *J. Neurosci.*, **20** (2000) 6672.
[6] Neiman A. and Russell D. F., *Phys. Rev. Lett.*, **86** (2001) 3443.
[7] Bahar S., Kantelhardt J. W., Neiman A., Rego H. H. A., Russell D. F., Wilkens L., Bunde A. and Moss F., *Europhys. Lett.*, **56** (2001) 454.
[8] Nawrot M. P., Boucsein C., Rodriguez-Molina V., Aertsen A., Grün S. and Rotter S., *Neurocomputing*, **70** (2007) 1717.
[9] Farkhooi F., Strube-Bloss M. F. and Nawrot M. P., *Phys. Rev. E*, **79** (2009) 021905.
[10] Peterson A. J., Irvine D. R. F. and Heil P., *J. Neurosci.*, **34** (2014) 15097.
[11] Avila-Akerberg O. and Chacron M. J., *Exp. Brain Res.*, **210** (2011) 353.
[12] Liu Y. H. and Wang X. J., *J. Comput. Neurosci.*, **10** (2001) 25.
[13] Chacron M. J., Longtin A. and Maler L., *J. Neurosci.*, **21** (2001) 5328.
[14] Prescott S. A. and Sejnowski T. J., *J. Neurosci.*, **28** (2008) 13649.
[15] Benda J., Maler L. and Longtin A., *J. Neurophysiol.*, **104** (2010) 2806.
[16] Schwalger T., Fisch K., Benda J. and Lindner B., *PLoS Comput. Biol.*, **6(12)** (2010) e1001026.
[17] Nesse W. H., Maler L. and Longtin A., *Proc. Natl. Acad. Sci. USA*, **107(51)** (2010) 21973.
[18] Farkhooi F., Muller E. and Nawrot M. P., *Phys. Rev. E*, **83** (2011) 050905.
[19] Urdapilleta E., *Phys. Rev. E*, **84** (2011) 041904.
[20] Schwalger T. and Lindner B., *Front. Comput. Neurosci.*, **7** (2013) 164.
[21] Shiau L., Schwalger T. and Lindner B., *J. Comput. Neurosci.*, **38** (2015) 589.
[22] Cox D. R. and Lewis P. A. W., *The statistical analysis of series of events* (Methuen & Co., Ltd., London) 1966.
[23] van Vreeswijk C., in *Analysis of parallel spike trains*, edited by Grün S. and Rotter S. (Springer-Verlag, Berlin) 2010, p. 3.
[24] Chacron M. J., Lindner B. and Longtin A., *Phys. Rev. Lett.*, **92** (2004) 080601.
[25] Lindner B., Chacron M. J. and Longtin A., *Phys. Rev. E*, **72** (2005) 021911.
[26] Prescott S. A., De Koninck Y. and Sejnowski T. J., *PLoS Comput. Biol.*, **4** (2008) e1000198.
[27] Mato G. and Samengo I., *Neural Comput.*, **20** (2008) 2418.
[28] Rauch A., La Camera G., Lüscher H. -R., Senn W. and Fusi S., *J. Neurophysiol.*, **90** (2003) 1598.
[29] La Camera G., Giugliano M., Senn W. and Fusi S., *Biol. Cybern.*, **99** (2008) 279.
[30] van Vreeswijk C. and Sompolinsky H., *Neural Comp.*, **10** (1998) 1321.
[31] Vogels T. P. and Abbott L. F., *Nat. Neurosci.*, **12** (2009) 483.
[32] Chacron M. J., Pakdaman K. and Longtin A., *Neural Comp.*, **15** (2003) 253.
[33] Hutcheon B. and Yarom Y., *Trends Neurosci.*, **23(5)** (2000) 216.
[34] Brown D. A. and Adams P. R., *Nature*, **283** (1980) 673.
[35] Nesse W. H., Del Negro C. A. and Bressloff P. C., *Phys. Rev. Lett.*, **101** (2008) 088101.
[36] Pozzorini C., Naud R., Mensi S. and Gerstner W., *Nat. Neurosci.*, **16** (2013) 942.
[37] Burkitt A. N., *Biol. Cybern.*, **95** (2006) 1.
[38] Madison D. V. and Nicoll R. A., *J. Physiol.*, **354** (1984) 319.
[39] Sah P., *Trends Neurosci.*, **19** (1996) 150.
[40] Muller E., Buesing L., Schemmel J. and Meier K., *Neural Comput.*, **19** (2007) 2958.
[41] Urdapilleta E., *Phys. Rev. E*, **83** (2011) 021102.
[42] Urdapilleta E., *J. Phys. A: Math. Theor.*, **45** (2012) 185001.
[43] Urdapilleta E., *J. Phys. A: Math. Theor.*, **48** (2015) 505001.
[44] Schwalger T. and Lindner B., *Eur. Phys. J. Special Topics*, **187** (2010) 211.
[45] Olver F. W. J., Lozier D. W., Boisvert R. F. and Clark C. W. (Editors), *NIST Handbook of Mathematical Functions* (Cambridge University Press, New York) 2010.